SANDIA REPORT
SAND2012-5658
Unlimited Release
Printed July 2012

DEVELOPMENT AND ASSESSMENT OF SOLAR-THERMAL-ACTIVATED FUEL PRODUCTION: PHASE 1 SUMMARY

James E. Miller, Mark A. Allendorf, Andrea Ambrosini, Eric N. Coker, Richard B. Diver, Ivan Ermanoski, Lindsey R. Evans, Roy E. Hogan, and Anthony H. McDaniel

Prepared by
Sandia National Laboratories
Albuquerque, New Mexico 87185 and Livermore, California 94550

Sandia National Laboratories is a multi-program laboratory managed and operated by Sandia Corporation, a wholly owned subsidiary of Lockheed Martin Corporation, for the U.S. Department of Energy's National Nuclear Security Administration under contract DE-AC04-94AL85000.

Approved for public release; further dissemination unlimited.

Sandia National Laboratories

Issued by Sandia National Laboratories, operated for the United States Department of Energy by Sandia Corporation.

NOTICE: This report was prepared as an account of work sponsored by an agency of the United States Government. Neither the United States Government, nor any agency thereof, nor any of their employees, nor any of their contractors, subcontractors, or their employees, make any warranty, express or implied, or assume any legal liability or responsibility for the accuracy, completeness, or usefulness of any information, apparatus, product, or process disclosed, or represent that its use would not infringe privately owned rights. Reference herein to any specific commercial product, process, or service by trade name, trademark, manufacturer, or otherwise, does not necessarily constitute or imply its endorsement, recommendation, or favoring by the United States Government, any agency thereof, or any of their contractors or subcontractors. The views and opinions expressed herein do not necessarily state or reflect those of the United States Government, any agency thereof, or any of their contractors.

Printed in the United States of America. This report has been reproduced directly from the best available copy.

Available to DOE and DOE contractors from
U.S. Department of Energy
Office of Scientific and Technical Information
P.O. Box 62
Oak Ridge, TN 37831

Telephone: (865) 576-8401
Facsimile: (865) 576-5728
E-Mail: reports@adonis.osti.gov
Online ordering: http://www.osti.gov/bridge

Available to the public from
U.S. Department of Commerce
National Technical Information Service
5285 Port Royal Rd.
Springfield, VA 22161

Telephone: (800) 553-6847
Facsimile: (703) 605-6900
E-Mail: orders@ntis.fedworld.gov
Online order: http://www.ntis.gov/help/ordermethods.asp?loc=7-4-0#online

SAND2012-5658
Unlimited Release
Printed July 2012

DEVELOPMENT AND ASSESSMENT OF SOLAR-THERMAL-ACTIVATED FUEL PRODUCTION: Phase 1 Summary

James E. Miller, Mark A. Allendorf, Andrea Ambrosini, Eric N. Coker, *Richard B. Diver, Ivan Ermanoski, Lindsey R. Evans, Roy E. Hogan, and Anthony H. McDaniel
Program Manager: Tony Martino

Sandia National Laboratories
P.O. Box 5800
Albuquerque, NM 87185

*Diver Solar, LLC
Albuquerque, NM

Abstract

Sandia National Laboratories has for many years been engaged in investigating and developing the science and technology of solar thermochemistry for solar fuel applications under the banner "Sunshine to Petrol." This report summarizes BP-funded solar thermochemical work performed from November 2011 through May 2012. This "phase one" effort centered on performance mapping of the Counter-Rotating-Ring Receiver Reactor Recuperator (CR5) prototype, a thermochemical heat engine for splitting CO_2 (and/or H_2O) to produce CO (H_2) and O_2. The bulk of the on-sun testing effort was performed with 8 ceria-finned rotating rings. During operation, argon is injected into the reduction side of the CR5 while CO_2 is provided to the oxidation side. Mixing of these two streams was characterized and it was confirmed that, while some degree of mixing does occur, the two sides are distinct from one another. For the chosen operating strategy crossover is principally from the reduction to the oxidation side. While testing, the CO and O_2 production rates exhibited a periodic behavior consistent with the ring rotation speed. This behavior results from non-uniform distribution of ceria, i.e. the number of fins in a given zone varies over time in a periodic fashion. This behavior is an indication that we are able to discriminate changes in gas composition over a very short time scale, provides verification that there are distinct oxidation and reduction zones in the system, and that the ceria is indeed responsible for the observed production of CO. In general, the CO yield increases with increasing reduction temperature and increasing CO_2 (and total) flow rate. The highest average CO yield at any run condition was 265 sccm. The efficiency significantly increases when the reduction temperature is increased from 1450 to 1550 °C. The increase is less pronounced when increasing the temperature to 1620 °C. The increased yields are offset by an increased power requirement. The highest average efficiency observed for any run condition was 0.66%. Analysis is ongoing. Possible strategies for improving the results include enhancing the rate of removal of gaseous products from the system, further minimizing gas crossover, and operating with a full complement of 22 rings.

TABLE OF CONTENTS

Table of Figures 6
Executive Summary 9
Introduction 13
Operation of CR5 with 22 Rings 13
Reactor & Materials Improvements Made to Improve Data Quality and Reduce Turnaround Time for CR5 14
Experimental Plan and Timeline for CR5 Performance Mapping 16
  Overview of Ring Fabrication 16
Execution of Experimental Plan 17
  Data Set 1 17
  Data Set 2a 21
  Data Set 2B 25
  Data Set 3 26
  Data Set 4 29
  Data Set 5 31
Solar Power Demands, Thermal behavior, Efficiencies 32
  Solar Calorimetry 32
  Thermal Behavior in Data Sets 2-5 33
  Solar Efficiencies 36
Other Resources 36
Acknowledgement 37

TABLE OF FIGURES

Figure 1. Selected data from 22 ring test conducted November 30, 2011. 13

Figure 2. Schematic of ring assembly (left) and photograph of an assembled ring with the bumper ring and common failure point identified (right) 15

Figure 3. Illustration of the steps involved in processing ceria tapes into ring segments. 17

Figure 4. Flows into and out of CR5. 18

Figure 5. Pressure/flow relationships when reactor pressure is allowed to float. Ar purge was constant at 1 SLPM, Ar and CO_2 flows were set to combinations of 16, 20, 24 and 20, 30, 40 SLPM for the respective streams. 18

Figure 6. CO_2 concentration in streams d (reduction outlet) and e (oxidation outlet) as a function of CO_2/Ar. Pressure is floating as in Figures 5. 19

Figure 7. Distribution of the total flow to streams d and e (left), and the distribution of CO_2 entering the reactor in stream c to streams d and e as reactor pressure is varied (right). Flows in = 9, 1, and 15 SLP in streams a, b, and c respectively (Figure 4). 20

Figure 8. Concentrations of Ar and CO_2 in streams d and e as a function of reactor pressure. Lines are provided as a benchmark and represent the perfect mixing scenario. Flows in are 9, 1, and 15 SLPM in streams a, b, and c respectively (CO_2/Ar = 1.5) 21

Figure 9. O_2 (black) and CO (red) concentrations in streams d and e respectively through the test day. 23

Figure 10. (left) Oxygen (black) and carbon monoxide (red) production through the test day, along with the ratio of the two (green) 23

Figure 11. (right) Production rate of CO plotted as a function of ring speed and CO_2 flow rate. Numerals on plot represent Order in which the points were collected. 23

Figure 12. Concentration of CO_2 in streams d and e as a function of CO_2/Ar ratio. Pressure and Ar flow held constant. 24

Figure 13. Oxidation temperature as a function of the nominal rotation speed and CO_2 flow (shown in legend). Ar flow=21 SLPM, TR= 1450 °C. 25

Figure 14. (left) Production rate of CO plotted as a function of ring speed and CO_2 flow rate 26

Figure 15. (right) Oxidation temperature as a function of the actual rotation speed and CO_2 flow (shown in legend). Ar flow=21 SLPM, TR= 1450 °C. 26

Figure 16. Example of data collected for Data Set 2. This particular plot corresponds to operating condition 3 in Table 1. 28

Figure 17. (left) Rate of CO production as a function of CO_2 flow rate and nominal rotation speed at thermal reduction temperatures of 1550 °C. Numerals represent the order in which the data was collected 29

Figure 18. (right) Oxidation temperature as a function of the actual rotation speed and CO_2 flow (shown in legend). Ar flow=21 SLPM, TR= 1550 °C. 29

Figure 19. (left) Rate of CO production as a function of CO_2 flow rate and nominal rotation speed at thermal reduction temperatures of 1550 °C. 30

Figure 20. (right) Oxidation temperature as a function of the actual rotation speed and CO_2 flow (shown in legend). Ar flow=21 SLPM, TR= 1550 °C. Pressure was allowed to float. 30

Figure 21. (left) Rate of CO production as a function of CO_2 flow rate and nominal rotation speed at thermal reduction temperatures of 1620 °C. 32

Figure 22. (right) Oxidation temperature as a function of the actual rotation speed and CO_2 flow (shown in legend). Ar flow=21 SLPM, TR= 1620 °C. 32

Figure 23. Calibration curves for "shaded' solar furnace. Top: Data Sets 2-4. bottom: Data Set 5 (see text.) 33

Figure 24. Actual reduction temperatures for Data Set 3. 34

Figure 25. (left) Temperature difference between reduction and oxidation sides of the cr5 as a function of Gas flow multiplied by the rotation period by data set. 35

Figure 26. (right) Power required to maintain the cr5 reduction temperature as a function of Gas flow divided by the rotation period by data set. 35

Figure 27. Efficiency as a function of CO_2 flow rate and period of a ring rotation for Data Sets 2b, 3, 4, and 5. 36

EXECUTIVE SUMMARY

This summary covers the entire phase 1 period of the project, which was initiated on November 9, 2011. To date, the following has been accomplished:

An on-sun evaluation of the CR5 was performed in November with a full complement of 22 rings (Jan 2012 report). This test was a follow-on to, and meant to validate, earlier 4 and 12 rings tests. The data was consistent with the earlier tests in the lower temperature regime. Data could not be collected at the extreme reduction temperature limit of 1650 °C due to a failure in a ring segment.

Following the 22-ring test, a new experimental plan, consistent with the statement of work, was outlined and provided to D. Cunningham for comment and verification (Jan 2102 report).

The first data set outlined in the experimental plan was collected under cold-flow (off-sun) conditions. There were two principal goals motivating this activity: (1) characterizing the mixing of the inert (argon) stream sweeping the thermal reduction zone with the CO_2 stream sweeping the oxidation zone as a function of independent reactor variables, and (2) determining whether the addition of the control valve between the CR5 and the oxidation side pump would allow the reactor pressure to be controlled.

Three complete on-sun data sets were collected with a single set of 8 rings. These tests were conducted over a period of several weeks and only minor maintenance (e.g. replacing damaged o-rings) was required between test periods. This allowed us to progress ahead of schedule.

- Nine run conditions (3 ring rotation speeds, three gas flow rates), 0.5 atm, reduction temperature of 1450 °C (Feb 2012 report);
- Repeat of the 1450 °C conditions (this is an addition to the test plan);
- Nine conditions (3 rotation speeds, three gas flow rates), 0.5 atm, reduction temperature of 1550 °C.

A fourth complete on-sun data set was collected with a new set of 8 rings. Two ring segments broke over the course of data collection, but fell clear and did not prevent completing the data set.

- Nine run conditions (3 rotation speeds, three gas flow rates), pressure allowed to float, reduction temperature of 1550 °C.

Following the collection of the fourth data set, the broken rings were replaced with rings fashioned from previously used segments. Three additional on-sun days were devoted to collecting data at a thermal reduction temperature of 1650 °C. We were successful only in collecting a partial data set due to unfavorable weather changes and a loss of electrical power to the system. Mechanical failures of the CR5 per se (i.e. ring breakage, melting of insulation, etc.) were not observed during any of the runs.

- Four conditions (3 rotation speeds at one flow rate, one additional flow and ring speed), 0.5 atm, reduction temperature of 1650 °C.

In support of the test plan and data analysis flowing water calorimetry was performed several times over the course of the project to characterize the power provided by the solar furnace as a function of attenuator position and normal incident radiation for the different configurations of

heliostat and concentrator. This data is required to accurately calculate the efficiency of the thermochemical process.

Prior to carrying out the test plan, improvements were made to the CR5 reactor to ensure its success and to improve the quality of data collected (see discussion in Jan and Feb 2012 reports).

- The analytical capability on the CR5 product streams was improved. This improvement allows us to better close the material balance (i.e. confirm the ratio of CO to O_2 in the products), thereby verifying that the chemistry is as claimed. The flow system downstream of the CR5 was simplified to decrease dispersive mixing, and to increase responsiveness. With these changes, periodic behavior, consistent with the ring rotation speed, became evident.
- A control valve was installed to allow the CR5 pressure to be controlled independently of the input flows, thereby simplifying experimental design and data analysis.
- A new interior was constructed to better accommodate an eight ring test.

Important observations, results, and learnings from this Phase 1 effort include:

- The cold-flow tests and previous experience prompted an operating strategy of high gas flow rates, high (near ambient) operating pressure, and an argon flow rate into the reduction side significantly exceeding the reduction side effluent.
- A fraction of CO_2 injected into oxidation zone crosses over to mix with the Argon injected into the reduction zone and vice versa. Complete mixing does not occur. For the given operating strategy crossover is principally from the reduction to the oxidation side.
- Periodic behavior is observed for the measured reactor temperatures, especially the reduction temperature. We attribute this behavior to the fact the pyrometer samples a fixed point in space through which rings and their attached fins are rotating.
- The CO and O_2 production is periodic with a period consistent with the ring rotation speed. This behavior results from the fact there are individual missing fins on the rings and they are not distributed in a uniform manner, therefore the number of fins in a given zone varies over time in a periodic fashion. This behavior is an indication that we are able to discriminate changes in gas composition over a very short time scale. Also, this behavior provides verification that there are distinct oxidation and reduction zones in the system, and that the ceria is indeed responsible for the observed production of CO.
- In general, the CO yield increases with increasing reduction temperature and increasing CO_2 (and total) flow rate. The highest average CO yield at any run condition was 265 sccm.
- The efficiency significantly increases when the reduction temperature is increased from 1450 to 1550 °C. The increase is less pronounced when increasing the temperature to 1620 °C. The increased yields are offset by an increased power requirement. The highest average efficiency observed for any run condition was 0.66%.
- The power required to maintain the reduction temperature increases with reduction temperature, the ring rotation speed and the total gas flow through the system. For a given reduction temperature the power correlates with the product of the gas flow rate and the ring rotation speed.
- Power demand is reduced when the reactor pressure is allowed to float at lower values. CO yields are also reduced so no advantage is realized.
- For a given reduction temperature, the oxidation temperatures increase with decreasing gas flows and increasing rotation speed. For a given data set the oxidation temperatures

correlate with the quotient of the gas flow and the rotation speed. The temperatures vary continuously through the oxidation zone and hence the temperature measurement is sensitive to pyrometer placement.

- At the lowest reduction temperature evaluated, 1450 °C, the process appeared to be limited by the rate at which O_2 was pumped from the system.
- Strategies for improving the results include enhancing the rate of removal of gaseous products from the system, further minimizing gas crossover, and operating with a full complement of rings.

A list of related references is provided on the final pages of this report.

INTRODUCTION

This report summarizes BP-funded solar thermochemical work performed from November 9, 2011 through May 2012. The work centered on performance mapping the Counter-Rotating-Ring Receiver Reactor Recuperator (CR5) prototype, a thermochemical heat engine conceived and built at Sandia National Laboratories. This Phase 1 work is presented largely in chronological order.

OPERATION OF CR5 WITH 22 RINGS

The CR5 was operated on November 30, 2011 with a full complement of 22 rings of the latest ceria fin design. The principle goal for the test was simply to collect a data set with full complement of rings to compare to and further validate earlier tests conducted prior to this Phase 1 effort with 4 and 12 rings. Prior to conducting this test, the oxygen sensor located in the thermal reduction side effluent was upgraded with the intent of allowing the material balance around CO_2 to be fully closed. Secondary goals included verifying that the new ceria fin design was robust, establishing and validating procedures for collecting data with improved O_2 sensor, validating that other improvements (new controls/flow meters) function as expected under on-sun conditions, and maximizing time–on-stream to build experience for newer members of the operations team. Finally, the tertiary goal was to establish a high efficiency mark if possible.

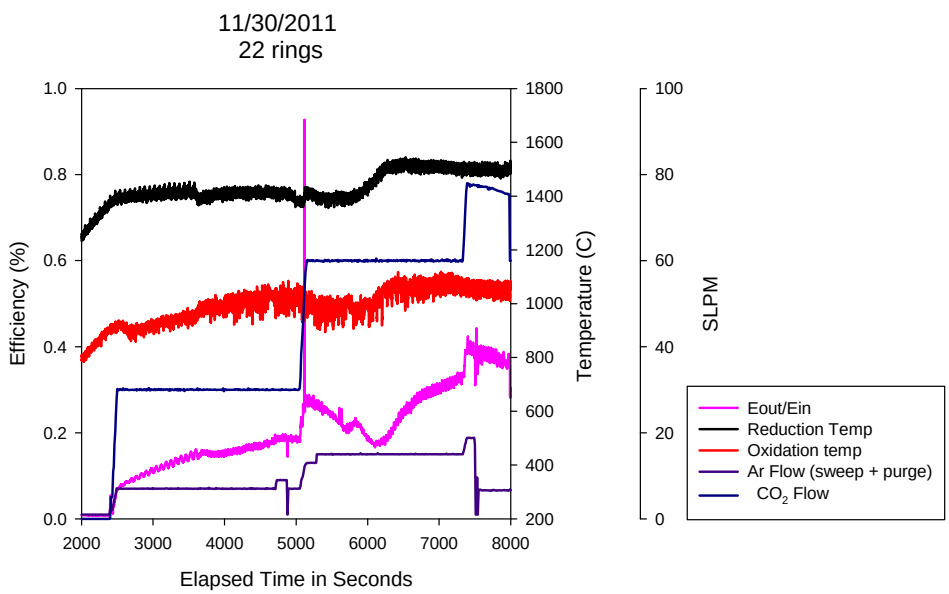

FIGURE 1. SELECTED DATA FROM 22 RING TEST CONDUCTED NOVEMBER 30, 2011.

During the course of the test, 47 different data signals were logged at one second intervals. Figure 1 illustrates how the independent variables of thermal reduction temperature and gas flows were varied over the course of the more significant portion of the test. The efficiency shown is calculated as the ratio of the heating value of CO exiting the oxidation side of the reactor to the solar flux into the system. Prior to the illustrated segment, calibrations were performed and verified, support systems (e.g. chilled water) were brought on-line and finally the system was brought on sun and slowly brought to temperature. When the thermal reduction temperature reached 1400 °C, the gas flows were brought on line and held steady (30 slpm CO_2, 7 slpm Ar). The efficiency increased over

time. Currently we attribute that increase to the slow increase in the oxidation temperature that it is seen to apparently track. The observation is consistent with laboratory data wherein optimum temperatures for CO production are > 1000 °C; at lower temperatures reaction rates are slow although thermodynamics are improved. The slow increase in the oxidation temperature is attributed to a slow increase in the system as a whole as it is thermally soaked. Notably when the flows were increased, the efficiency also increased. This has been observed in the past and was tentatively attributed to an increase in the reactor pressure, although performance mapping revealed similar behavior at fixed pressure, seemingly negating this interpretation. The subsequent loss of efficiency is unexplained but again may be attributable to the decrease in the oxidation temperature that was observed. (Increased flows decrease the oxidation temperature – see below.) As expected in the final two operational variations, efficiency improved when the reduction temperature was increased and as the gas flow were once again increased.

Operations were ceased shortly after the illustrated time frame. Two observations hastened this decision: 1) The flow out of the reduction side pump became severely limited, and 2) Several of the rings being remotely monitored by video ceased to rotate. Post-operation analysis revealed the reasons for these events to be 1) temperature of the reduction side effluent was high and thus the mass flow through the pump was limited (this was verified in subsequent flow testing), and 2) cracking/separation of zirconia wedge segments at or near the metal/zirconia connection point dislodged the rings from their drives. These observations prompted several of the changes discussed below.

Despite the earlier than anticipated shutdown, several useful observations were made. First, the new O_2 sensor improved but did not result in the ability to fully close the material balance around reacted CO_2 (i.e. $CO \neq 2\ O_2$). Material balances on other species (the unreacted CO_2 and Ar) indicated that there was significant degree of cross-over between zones, particularly at the lower flow rates (lower pressures). These observations prompted the inclusion of analytical capacity (gas chromatographs) as well as the repositioning of the control valves to enable better control of reactor pressure independent of flow rate. Regarding the comparison to the earlier tests, the data is similar when scaled by the number of rings. Unfortunately, the comparison could not be made at thermal reduction temperatures in the vicinity of 1650 °C where the highest and most tantalizing efficiencies were observed in the earlier tests.

REACTOR & MATERIALS IMPROVEMENTS MADE TO IMPROVE DATA QUALITY AND REDUCE TURNAROUND TIME FOR CR5

Following the 22-ring test, the CR5 was disassembled and the rings and ring segments recovered for reuse. It was determined at this stage that a number of improvements should made to the CR5 and associated systems to improve the quality of the data being collected and to increase the ruggedness and operability of the system thereby eliminating or greatly reducing unwanted shutdowns, thereby reducing the turnaround time between on-sun tests. Regarding the data quality, the ability to reliably collect concentration and flow data of sufficient quality that the material balances could be closed was a particular driving concern. The specific following improvements were made.

Water condensers on both exit streams (oxidation and reduction chambers) were removed. Condensers are not required for the current focus on CO_2 splitting. Eliminating these subsystems removed a significant volume "capacitance" from the system. As a result, the analytical instruments were more responsive to changes in reactor operating conditions (less time lag, sharper response). A further advantage was that this change allowed a pressure control valve to be closely coupled to the CR5 body in the oxidation side effluent stream. This was later shown to enable effective pressure control. The condensers can be reinstalled at a later date as part of switchover to steam operation if desired. However, modifications will be required if pressure control valves are to remain in place.

A new ring drive was designed and fabricated. The design that was implemented at the time of the 22-ring test included gears only to drive the rings; the rings themselves "rode" or "floated" on a guide cylinder. This avoided issues encountered with idler gears, but allowed for some side-to-side motion and created the potential for derailing and seizure. The new design throughout the remainder of Phase 1 included idler gears for each ring that are mounted on guide rods. The guide rods themselves are actively water cooled during operation (each rod is a tube-in-tube design with flow through the inner tube and annular space) so that the temperature can be maintained at a temperature consistent with favored lubricants. Additionally, the idler gears are positioned so that the tension is adjustable.

The bumper rings were modified. The bumper ring is the metal ring that contains the gear teeth and holds the ceramic subassemblies in place (See Figure 2). In several cases, including the 22-ring test, failures of individual ring segments occurred in the vicinity of the ceramic-metal interface. Post test evaluation indicated high stress at this point due to differential expansion of the inner and outer perimeters of the bumper (i.e., upon disassembly the bumpers tended to distort into a cup shape). Radial kerfs were cut in these rings to relieve the accumulated stress. Subsequently fewer failures occurred at this point, although other factors may also have contributed to the improvement.

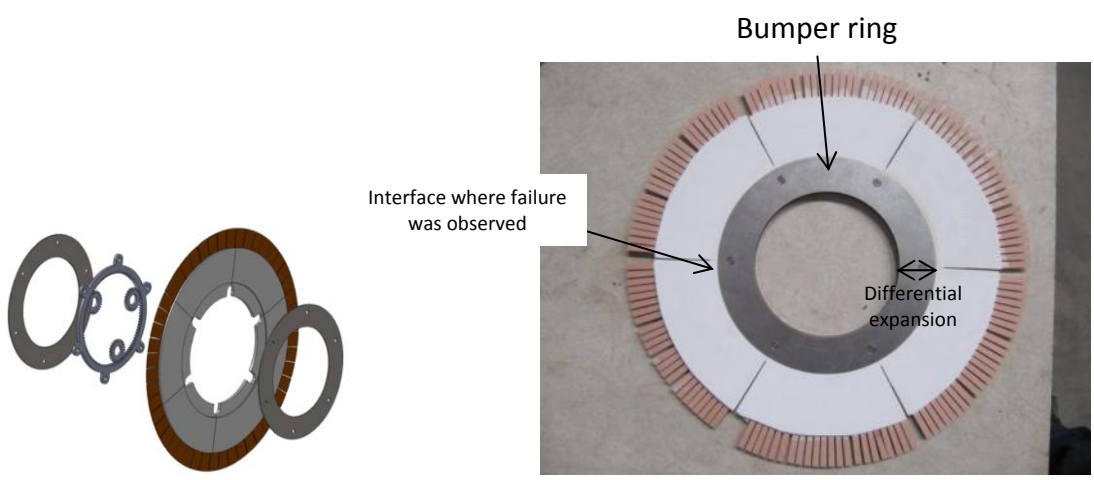

FIGURE 2. SCHEMATIC OF RING ASSEMBLY (LEFT) AND PHOTOGRAPH OF AN ASSEMBLED RING WITH THE BUMPER RING AND COMMON FAILURE POINT IDENTIFIED (RIGHT).

The on-line analytical capability was significantly upgraded and redundancy was added. As indicated above, the oxygen sensor initially installed on the reduction side effluent proved to be

particularly susceptible to drift under operating conditions. Therefore, prior to the 22-ring test, this sensor was replaced with an Ametek instrument electrochemical type sensor. The results were much improved with this sensor; however the device was known to be sensitive to CO, thus crossover of CO from the oxidation side could be expected to skew the results. Although this could be corrected for, we added micro-gas chromatography capability to both reduction and oxidation effluent. These instruments have a sampling rate of only one to several minutes but effectively supplement and verify the more specific NDIR and oxygen sensors (sampled at 1 second intervals). Additionally, the GC capability allows the quantification of products and reactants that may have crossed over from their target zones. With the complete analytical set operational, we could analyze for all of the reactive components potentially present (CO_2, CO, and O_2) in each gas stream exiting the reactor. In addition to the chemical analysis, flow sensors with broader range were added to effluent streams, and flow meters with broader range and better operating characteristics at sub-ambient pressures were installed. All of these devices, with the exception of the GCs, were integrated into the lab-view control and data acquisition system. With these improvements and refined techniques, the ability to able to close material balances to within 10% was demonstrated in cold-flow tests with representative gas mixtures.

A heat exchanger was added to cool the gas exiting the thermal reduction side. This addition prevents loss of mass flow through the pump and also prevents thermal damage to the pump.

EXPERIMENTAL PLAN AND TIMELINE FOR CR5 PERFORMANCE MAPPING

An experimental plan consistent with the negotiated Statement of Work and available time-frame and resources was formulated and provided to BP in January. The overall goal of the plan was not to maximize the performance of the system, but rather to collect enough data to create a performance map of the system suitable for validating models and guiding future improvements. Four distinct data sets were to be collected. Data Set 1 was to be comprised of cold flow data with the goal of establishing operating conditions for the other data sets. In particular the amount of crossover (e.g. the CO_2 flowing from the oxidation side to the reduction side of the CR5) was to be determined as a function of Ar/CO_2 flows into the reactor. The cold tests were also to verify that the modifications made to the system would enable pressure control within the CR5 as planned. The target date by which Data Set 1 was to be collected was February 13, 2012.

The target date for Data Set 2 was March 15, 2012. Data Set 2 was to consist of a total of nine on-sun steady-state data points with 8 ceria-finned rings (3 ring rotation speeds, 3 CO_2 flow rates, Ar flow fixed, $T_{reduction}$ = 1450 °C, fixed pressure if possible). Data Set 3 was to be similar with the thermal reduction (TR) temperature increased to 1550 °C. A decision point followed Data Set 3. Based on the eariler results, rings remaining in inventory, etc., Data set 4 was to either be similar to Data Set 3 with a full complement of 22 rings, or similar to Data Set 3 with the TR temperature set to higher than 1600 °C.

OVERVIEW OF RING FABRICATION

During Phase 1, an existing inventory of cast ceria was processed and converted from green tapes to fins (Figure 3). This involved cutting the tapes into strips, die cutting into squares, hand stacking

and aligning the squares 12 thick, vacuum packing and hot pressing to form laminates, laser cutting the laminates (each square provides 4 fin subset), and finally transferring the green laser cut laminates and firing to a predetermined schedule. This effort combined with the inventory on hand provided fin materials for as many as 44 complete rings for the performance mapping exercise, not accounting for potential reuse of used segments.

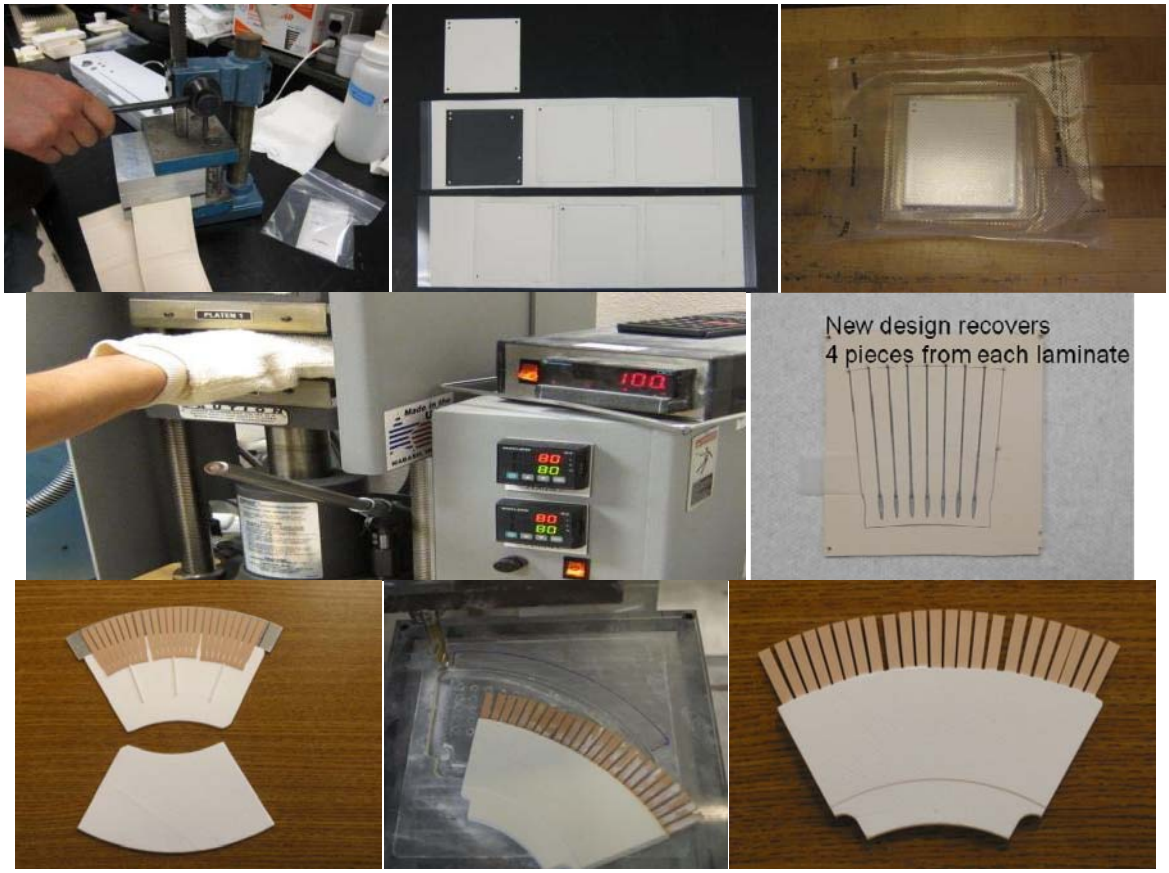

FIGURE 3. ILLUSTRATION OF THE STEPS INVOLVED IN PROCESSING CERIA TAPES INTO RING SEGMENTS.

EXECUTION OF EXPERIMENTAL PLAN

DATA SET 1

There were two principal goals motivating data set one: (1) characterize the mixing of the inert (argon) stream sweeping the thermal reduction zone with the CO_2 sweeping the oxidation zone as a function of independent reactor variables, and (2) determine whether the addition of the control valve between the CR5 and the oxidation side pump would allow reactor pressure to be controlled.

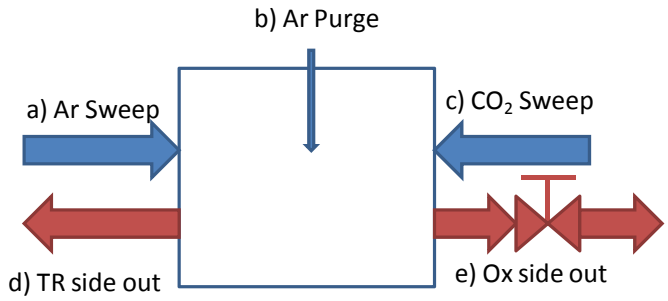

FIGURE 4. FLOWS INTO AND OUT OF CR5.

For clarity, Figure 4 illustrates the mixing scenario. There are three gas streams fed into the CR5 chamber: (a) the Ar sweep flowing into the reduction side, (b) the small Ar purge used during pump down and to sweep reactive gasses from the central cavity (inside the stack of rings) during operation, and (c) the CO_2 sweep/reactant flowing into the oxidation side. There are two streams flowing out through vacuum pumps (not shown): (d) the thermal reduction side out, and (e) the oxidation side out. The pressure control valve is positioned on stream (e), between the CR5 and the pump; the pressure measured in the CR5 is manipulated by regulating the flow in stream (e).

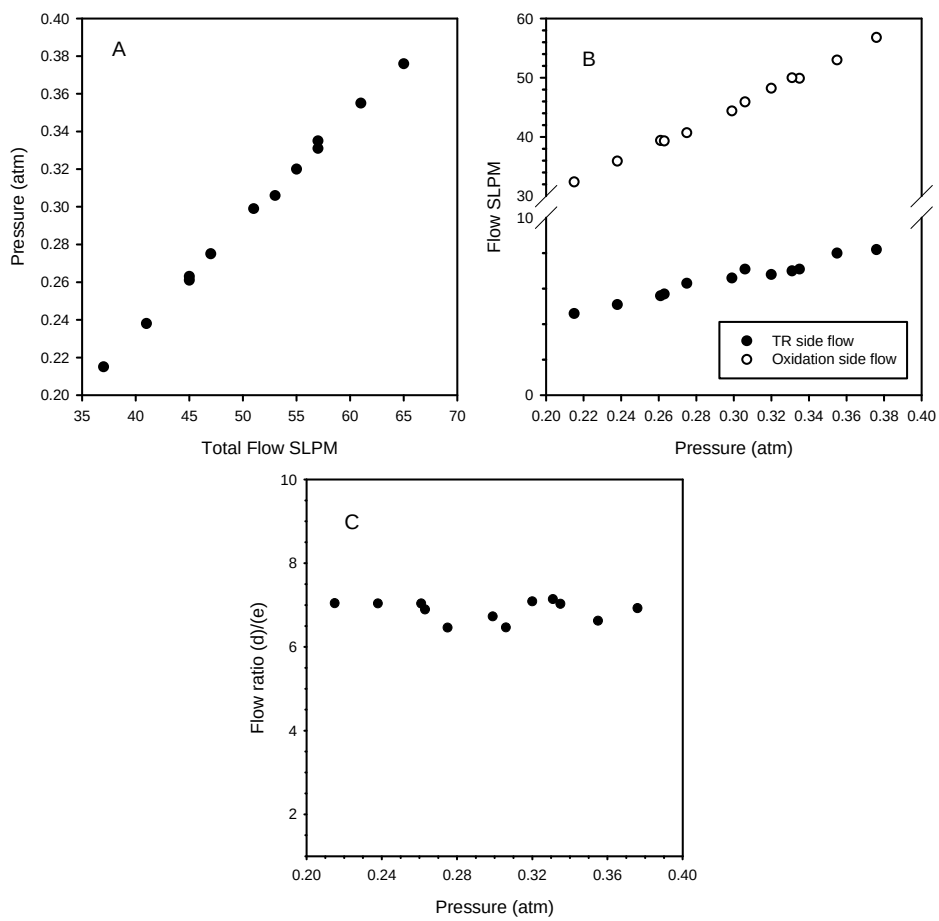

FIGURE 5. PRESSURE/FLOW RELATIONSHIPS WHEN REACTOR PRESSURE IS ALLOWED TO FLOAT. Ar PURGE WAS CONSTANT AT 1 SLPM, Ar AND CO_2 FLOWS WERE SET TO COMBINATIONS OF 16, 20, 24 AND 20, 30, 40 SLPM FOR THE RESPECTIVE STREAMS.

Prior to installation of this valve, the reactor pressure was allowed to float. That is, the reactor established an equilibrium pressure based on the inlet flows and the pumping capacities of the two vacuum pumps. Figure 5A illustrates the cold pressure in the CR5 as a function of total flow while Figure 5B illustrates the distributions of the flow out of the reactor as a function of total pressure. Figure 5C shows the ratio of the two data sets plotted in 5B. The pumping speeds are not variable, thus as one might expect, the flows out of each side are dependent only on pressure and not on the distribution of the flows, and the ratio of the flows in (d) and (e) is constant. That is, the flows in streams (d) and (e) respond only to the variable (a+b+c), not to a variable such as (c/a). Therefore, increasing the Ar sweep flow rate only increases the flow out of the TR reduction side in a manner proportional to the total pressure, not to the ratio of Ar to CO_2 entering the reactor.

This point is further reinforced in Figure 6 wherein the concentration of CO_2 in streams d and e is plotted as a function of the ratio of CO_2 flow (c) to Ar flow (a+b). The solid line provided for comparison is simply the concentration of CO_2 that would result from perfect mixing of streams (a), (b), and (c). One can think of the difference between any point and the line as a measure of how much mixing is occurring. This figure makes it clear that the streams exiting the oxidation side are very well mixed, while a fair degree of separation is maintained on the reduction side. This is the result of the fact that the argon flow into the reactor in all cases exceeds the pumping speed on the reduction side. Hence there is a net flow of Ar away from the reduction side and mixing necessarily occurs on the oxidation side. Since a large percentage of the total flow exits the system through the oxidation side, this accounts for the close correlation between the CO_2 concentration on the oxidation side and the complete mixing curve.

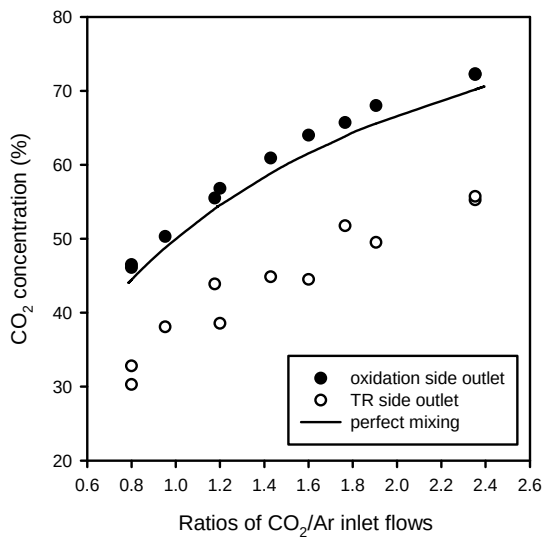

FIGURE 6. CO_2 CONCENTRATION IN STREAMS D (REDUCTION OUTLET) AND E (OXIDATION OUTLET) AS A FUNCTION OF CO_2/Ar. PRESSURE IS FLOATING AS IN FIGURES 5.

Taken as a whole, Figures 5 and 6 suggest that there is little effect of the total flow rate (or operating pressure) on mixing. Additionally the ratio of CO_2 to Ar seems to have a relatively small impact on the "degree" of mixing as measured against complete mixing. It is unclear from Figure 6 if it is preferable to maximize the CO_2 on the oxidation side where it will enhance kinetics, or minimize it on the reduction side where it may negatively influence the thermodynamics (at high enough temperatures, CO_2 can be considered inert in the reduction side).

Figure 7 presents data wherein the total flow was maintained at 25 SLPM (9, 1, and 15 SLPM in streams a, b, and c, respectively) while the pressure control valve was manipulated to increase the reactor pressure. Figure 7A shows the distribution of flow out of the reactor between stream (d) and (e). As the pressure is increased (i.e., the flow to (e) is restricted), a larger fraction of the total flows out of the reduction side. The amount of CO_2 flowing in streams (d) and (e) is illustrated in Figure 7B. The CO_2 concentration in each stream was determining by GC analysis. The sum of the two flows relative to 15 SLPM is indicative of the material balance. The data in 7B mirrors that in 7A – more CO_2 flows to the reduction side as the reduction side total flow increases.

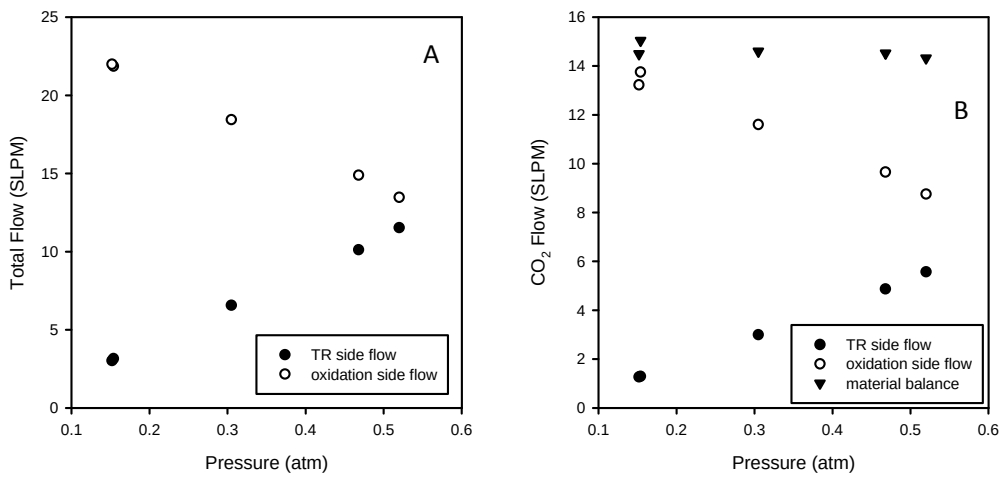

FIGURE 7. DISTRIBUTION OF THE TOTAL FLOW TO STREAMS D AND E (LEFT), AND THE DISTRIBUTION OF CO_2 ENTERING THE REACTOR IN STREAM C TO STREAMS D AND E AS REACTOR PRESSURE IS VARIED (RIGHT). FLOWS IN = 9, 1, AND 15 SLP IN STREAMS A, B, AND C RESPECTIVELY (FIGURE 4).

Figure 8 illustrates the distribution of CO_2 and Ar in each of the streams exiting the reactor, (d) and (e). The solid lines are the Ar (black) and CO_2 (red) concentrations that would result from complete mixing. As in the case when the pressure was allowed to float, the composition in the reduction stream (d) is fairly enriched in Ar relative to perfect mixing, while being less so in stream (e) (oxidation). As the pressure is increased and more flow is directed into stream (d), it becomes less enriched in Ar. Note that at the highest pressures however, the total flow in stream (d) exceeds the flow of Ar into the system (a+b), hence mixing is necessarily expected to occur.

To summarize, in all cases significant degrees of mixing were observed. However, stream (d) (thermal reduction exit) was significantly enriched in Ar relative to the perfect mixing standard. The reactor pressure has very little effect on the degree of mixing. However, as should be expected, for a given flow combination there is a greater degree of mixing in stream (d) as the flow of that stream approaches and exceeds the total Ar flow into the reactor (a+b). From an operations standpoint we believe there is a tradeoff in the reactor operating pressure: lower pressures should favor the thermal reduction (from an equilibrium standpoint), while higher pressures favor the oxidation kinetics (but not the thermodynamics). Testing performed up to this date indicates that the best results (highest efficiencies) were obtained when the total flow rate, and hence the operating pressure, was high (approaching ambient pressure, 630 Torr in Albuquerque). Taking this into account with the data presented here would suggest an operating strategy wherein the pressure is maintained at a relatively high level and the Ar flow significantly exceeds the flow exiting the thermal reduction side (d).

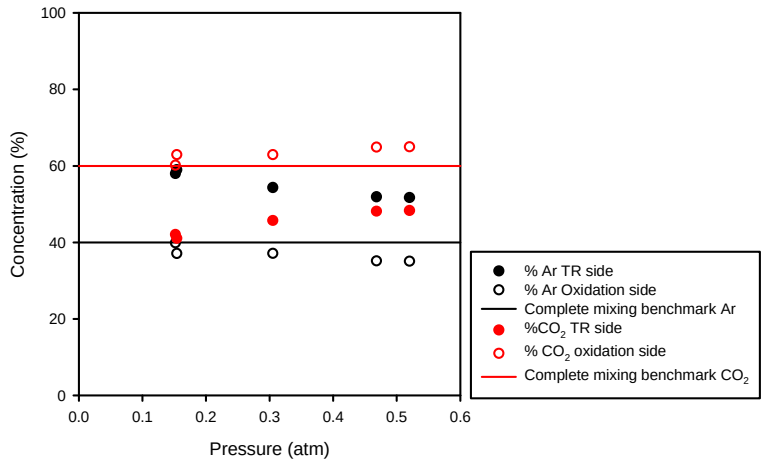

FIGURE 8. CONCENTRATIONS OF AR AND CO_2 IN STREAMS D AND E AS A FUNCTION OF REACTOR PRESSURE. LINES ARE PROVIDED AS A BENCHMARK AND REPRESENT THE PERFECT MIXING SCENARIO. FLOWS IN ARE 9, 1, AND 15 SLPM IN STREAMS A, B, AND C RESPECTIVELY (CO_2/Ar = 1.5).

DATA SET 2A

The first on-sun campaign to collect operational data for Data Set 2 began on Saturday, February 25, 2012. As planned, the experiments were performed in an 8-ring configuration. The test plan called for maintaining the thermal reduction temperature at a constant value of 1450 °C, maintaining the Ar flows at 20 SLPM (stream a) and 1 SLPM (b), and maintaining the reactor pressure at 0.5 atm. As the flow out of the reduction side (stream d) is approximately 10-11 SLPM at this pressure, this combination is consistent with the reasoning outlined in the discussion of Data Set 1. The CO_2 flows were to be varied to three different values, as was the ring speed to create a matrix of 9 operating conditions. The order in which the 9 data points were to be collected was randomly chosen and is shown in Table 1.

TABLE 1. OPERATING CONDITIONS FOR DATA SET 2A.

Operating Condition	CO_2 Flow (SLPM)	Ring Speed (RPM)
1	40	0.9
2	30	0.9
3	20	1.2
4	30	0.6
5	30	1.2
6	40	0.6
7	40	1.2
8	20	0.6
9	20	0.9

On the morning of the test, the instruments were calibrated and the TR temperature was slowly brought to 1000 °C under an Ar purge of 1 SLPM. The CR5 was allowed to soak at this temperature and then the temperature was raised to 1450 °C. As this temperature was approached flows were

initiated and brought to the values outlined for Condition 1. The TR temperature was measured by a pyrometer (1.39 micron) focused near top-dead-center on the central rings 4 and 5. It is important to keep in mind that the temperatures vary continuously throughout the reactor as the rings spin into and out of the hot zone, and that this temperature is something of a rough average measure. The protocol that was followed called for the first condition to be maintained for at least 40 minutes and the following conditions to be maintained for at least 20 minutes. These were to be extended in cases where observable variables (e.g. oxidation temperature) were not judged to be constant over a period of at least 10 minutes. In general this was only necessary for the lowest rotation speeds. The individual values presented from this point in the report forward for variables such as temperatures, pressures, gas production rates, etc…, are representative averages over the last 10 minutes of run at each condition (the steady-state period), unless otherwise stated.

Mechanically, this test was by far the most successful performed up to that date. The reactor was maintained at 1450 °C for almost 4 hours, with the test day ending only when we could no longer maintain that temperature due to the decreasing sunlight late in the day. No mechanical failures were observed and the rings continued to spin reliably throughout the day and after the reactor was cooled. As viewed through the aperture, the spinning rings appeared to have suffered only the loss of three small fin sections. Upon cooling several o-rings downstream of the main CR5 did fail (leak), as they had suffered thermal damage. These were easily replaced without removing the assembly from the test stand. The test was also very successful from the point of view of collecting steady-state data and in meeting the goals of the test plan. Data was collected for each of the 9 conditions. Throughout the run time, 53 individual data points (many of which are temperatures collected for modeling and troubleshooting purposes) were logged at one second intervals for over 20,000 seconds. GC data was collected over the same time period at several minute intervals.

Figure 9 is an overview of the run showing the concentrations of O_2 and CO in streams (d) and (e), respectively, over the course of the data collection period. The concentration of O_2 (Ametek sensor) in the gas exiting the thermal reduction side exhibited relatively little variation over time compared to the CO concentration (NDIR) in the gas exiting the oxidation side. The variations in CO concentration correlated inversely with CO_2 inlet flow rate. The corresponding volumetric flow rates of O_2 and CO in streams (d) and (e) respectively are plotted in Figure 10 along with the ratio of the two. Average values extracted from the latter portion of each run condition are presented in Figure 11.

Figures 10 and 11 show that the concentration/flow dynamic yielded CO and O_2 production rates that were surprisingly consistent across nearly all run conditions, with the exception of the first two data points collected. The CO and O_2 flow rates are determined as the products of the concentrations and total volumetric flows in each stream. As expected, the reduction side outlet flow rate was essentially constant over the course of the day (~11 SLPM) as it varies only with pressure, which was held constant (actual pressure varied between 0.5-0.56 atm). The flow exiting the oxidation side increased with increasing CO_2 flow and as the control valve was opened to maintain the pressure. Thus the lower concentrations were compensated for by higher flows out in the oxidation side outlet.

The steady state ratio of CO to O_2 averages roughly 2.2 (Figure 10) across the last seven conditions, within the margin of error for our material balance. Also, the GC data verifies very little realized crossover of CO into stream (d), and of O_2 into stream (e). This is not unexpected as these species would be likely to react with each other as they cross over, producing CO_2. The CO:O_2 ratio is

anomalously high during the portions of the operation corresponding to data points 1 and 2. We suspect that this anomaly resulted from the fact that new materials (e.g. insulation) had been installed in the reactor and that these generally can be expected to offgas some remnants of hydrocarbon contamination until they have been "burned in". In support of this assumption, we note that we detected anomalous GC peaks during the heat-up phase although these were largely eliminated prior to reaching reaction temperature and collecting data. The anomalous peaks were not detected in subsequent runs.

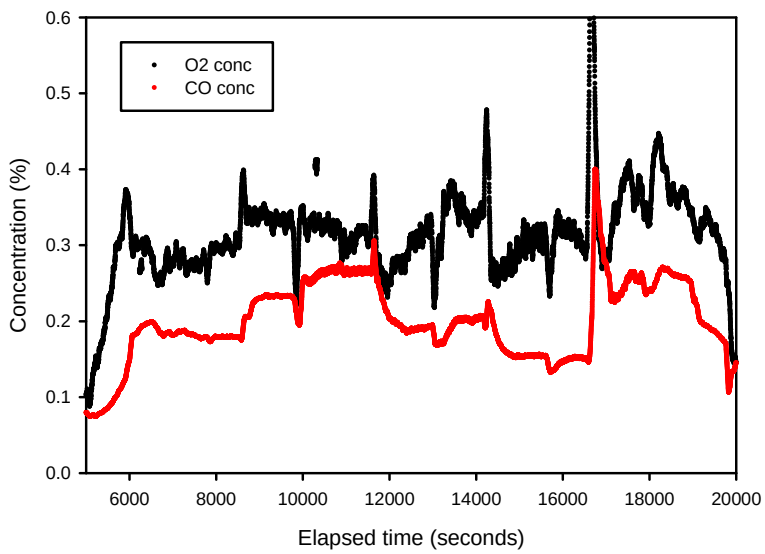

FIGURE 9. O_2 (BLACK) AND CO (RED) CONCENTRATIONS IN STREAMS D AND E RESPECTIVELY THROUGH THE TEST DAY.

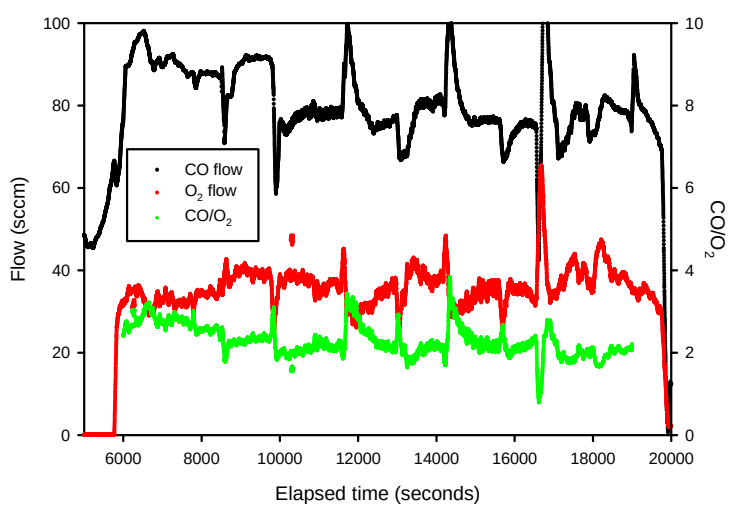

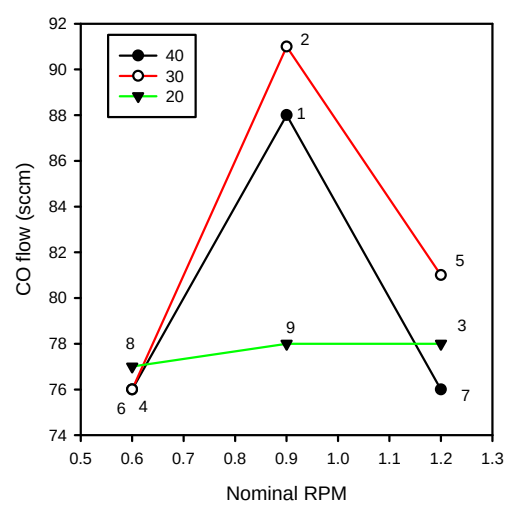

FIGURE 10. (LEFT) OXYGEN (BLACK) AND CARBON MONOXIDE (RED) PRODUCTION THROUGH THE TEST DAY, ALONG WITH THE RATIO OF THE TWO (GREEN).

FIGURE 11. (RIGHT) PRODUCTION RATE OF CO PLOTTED AS A FUNCTION OF RING SPEED AND CO_2 FLOW RATE. NUMERALS ON PLOT REPRESENT ORDER IN WHICH THE POINTS WERE COLLECTED.

The small degree of variation in the CO production (less than 20% from highest to lowest) with changes in rotation speed and gas flows (Figures 9, 10, and 11) was not expected but suggest there is a common controlling element to all cases. Possibilities include reaction kinetics, thermodynamic equilibria, and mass transfer (diffusion in gas and solid, and bulk flows of solid and gas). The limiting factor could occur on either the oxidation or reduction side of the reactor. Yet, it seems unlikely that the limiting factor occurs during oxidation as the temperatures and gas flows vary on the oxidation side with operating condition. Conversely, the oxygen concentration and flow is very consistent on the reduction side pointing to the reduction process as the limiter. As the temperature is constant and the results are somewhat independent of rotation rate (ceria mass flow), we tentatively propose that the conversion in this case may be limited by an equilibrium coupled to the rate at which oxygen is being pumped out of the reactor. That is, we suggest that at all conditions the reaction process is limited not by a dynamic process associated with the solid, but rather by rate at which oxygen can be removed from the reactor. I.e., as the pumping speed is constant across conditions, the production rate is likewise constant. If this interpretation is accurate it suggests a possible path to improvement to be found in increasing the rate at which O_2 is removed from the system, and or decreasing the oxygen partial pressure.

Mixing data similar to Figure 6 for Data Set 1 is provided for Data Set 2 in Figure 12. The data verifies that mixing is less pronounced on the reduction side than on the oxidation side and seemingly at smaller ratios of CO_2:Ar. Note that the amount of CO_2 in stream (d) is lower than that observed in Figure 6 under similar conditions (CO_2/Ar = 1.5, P=0.5 atm), seemingly validating our decision to increase the overall Ar flow.

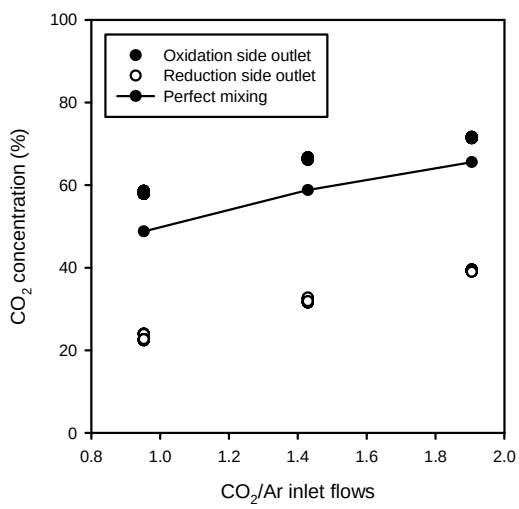

FIGURE 12. CONCENTRATION OF CO_2 IN STREAMS D AND E AS A FUNCTION OF CO_2/AR RATIO. PRESSURE AND Ar FLOW HELD CONSTANT.

Finally, Figure 13 shows the temperature measured on the oxidation side of the CR5 as a function of ring rotation speed and CO_2 flow rate. Throughout the run day, variables such as the temperature measured by the pyrometer and the gas concentrations were observed to periodically cycle through a small range. The concentrations in particular displayed a periodicity consistent with the rotation speed. The amplitude also varied as the conditions were varied. As noted above, the values in Figure 13 represent an average over the final 5-10 minutes of each test condition. Slower ring rotation and higher gas flows resulted in lower temperatures. This is consistent with increased transport of heat out of the reactor per unit rotation at higher gas flows as well as the expectation

from modeling that ring to ring radiative heat transfer (recuperation) will improve with decreased ring speed. Unfortunately an error in the data collection system prevented the solar furnace attenuator position from being recorded. Therefore the solar power input corresponding to each data point in the figure cannot be precisely determined.

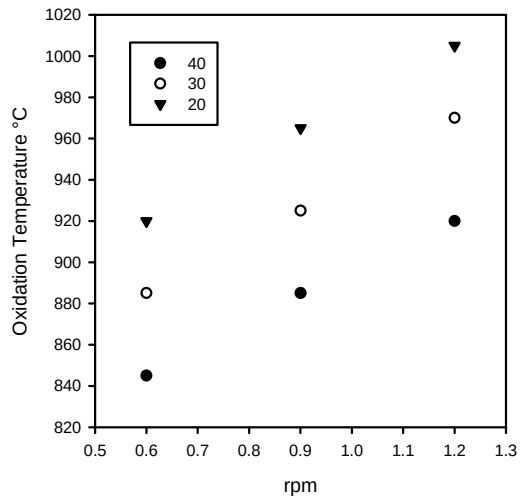

FIGURE 13. OXIDATION TEMPERATURE AS A FUNCTION OF THE NOMINAL ROTATION SPEED AND CO_2 FLOW (SHOWN IN LEGEND). Ar FLOW=21 SLPM, TR= 1450 °C.

DATA SET 2B

Data Set 2B, collected in March, was a replicate confirmation of Data Set 2A. The data was collected using the same set of rings from the earlier test; in the interim between collecting sets 2 and 3, the reactor was brought to temperature but data collection was pre-empted by a change in weather. Also in the interim, minor maintenance (e.g. replacement of o-rings) was performed. Given the seemingly anomalous data for the first two run conditions in Data Set 2A, the order of data collection was altered to see if a similar phenomenon was observed (Table 2).

TABLE 2. OPERATING CONDITIONS FOR DATA SET 2B.

Operating Condition	Ar Flow (SLPM)	CO_2 Flow (SLPM)	Nominal Ring Speed (RPM)
1	20	20	0.9
2	20	20	0.6
3	20	30	0.9
4	20	40	0.9
5	20	40	1.2
6	20	40	0.6
7	20	30	1.2
8	20	30	0.6
9	20	20	1.2

A plot comparable to Figure 11 is provide as Figure 14 and a plot similar to 13 is provided as Figure 15. Figure 14 shows that the CO yields are less than those observed for Data Set 2A. Also, the

higher yields observed for conditions 1 and 2 in Data Set 2A were not repeated for the same conditions (4 and 3) in Data Set 2B. The oxygen sensor failed to operate reliably during the data collection period, however the GC data is consistent with reduced yields. The difference in CO yields is at least partially attributable to the breakage/loss of some of the individual fins, during the two operations. However, post test inspection did not indicate as large a loss of fins as might be inferred from the difference in the data. An alternate explanation is that the operating conditions although similar, were not identical. In support of this rationale, we point to the oxidation temperatures recorded for Data Set 2B (Figure 15). Although the measured thermal reduction temperature (1450 °C) was similar in both cases, the oxidation temperatures recorded for this replicate data set are higher by roughly 100 °C. Countering this rationale is the fact that an examination of the temperatures of the gas streams exiting the CR5, which average over a larger area, were very similar for the two cases.

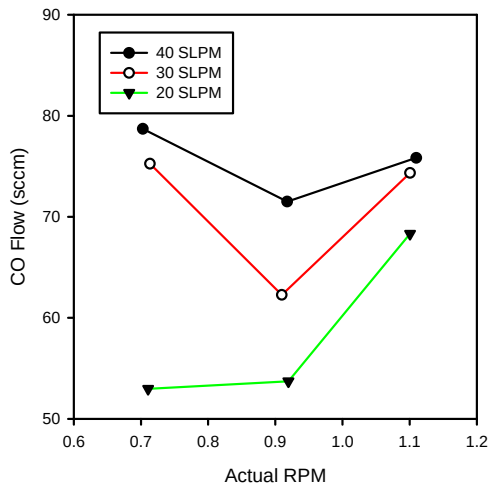

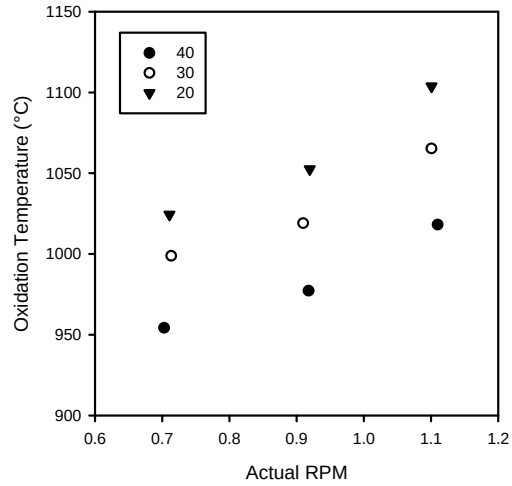

FIGURE 14. (LEFT) PRODUCTION RATE OF CO PLOTTED AS A FUNCTION OF RING SPEED AND CO_2 FLOW RATE.

FIGURE 15. (RIGHT) OXIDATION TEMPERATURE AS A FUNCTION OF THE ACTUAL ROTATION SPEED AND CO_2 FLOW (SHOWN IN LEGEND). Ar FLOW=21 SLPM, TR= 1450 °C.

The discrepancy in the oxidation temperatures is likely due to the fact that the reported values are more representative of point, rather than average, measurements. To elaborate, the temperatures in the CR5 are monitored via optical pyrometers which sample a relatively small section of the rotating rings. This occurs in the context of a device wherein the temperatures of the fins are understood to vary continuously along the path of rotation, and from ring to ring. Hence, small variations in the aiming of the pyrometers and in reactor location as the CR5 is moved to perform maintenance can lead to variations in the measured temperature. Thus the pyrometer temperatures should be understood as representative benchmarks for operation and as relative measures rather than as perfect absolute measures.

DATA SET 3

Data Set 3 consists of a similar set of flow and rotation conditions as Data Sets 2 (Table 3), with the thermal reduction temperature increased to 1550 °C. The data was collected on March 14 using the same set of rings used to collect Data Sets 2. As before, the pressure was held constant at 0.5 atm,

which fixed the flow out of the thermal reduction side of the CR5 at ~11 SLPM. The start-up and operating protocol were similar to those outlined above. The reactor was maintained at 1550 °C for over 4 hours with data collected for each of the 9 conditions. No mechanical failures occurred, and the rings continued to spin reliably throughout the day and after the reactor was cooled, although some irregular movement was observed late in the day and in the cooled state.

TABLE 3. OPERATING CONDITIONS FOR DATA SET 3.

Operating Condition	Ar Flow (SLPM)	CO_2 Flow (SLPM)	Nominal Ring Speed (RPM)
1	20	40	1.2
2	20	40	0.9
3	20	30	0.9
4	20	40	0.6
5	20	20	0.9
6	20	30	1.2
7	20	30	0.6
8	20	20	1.2
9	20	20	0.6

Figure 16 gives an example of data collected for one of the operating conditions (condition 3 in Table 3). Data was recorded at 1 second intervals. As mentioned above, the recorded temperatures vary in a somewhat periodic fashion and over a reasonably broad band. In particular the thermal reduction temperature varies over roughly a 60 °C range. Again, we attribute this variability to the fact the pyrometer samples a fixed point in space through which rings and their attached fins are rotating.

The data for the CO concentration (blue points) is periodic with the length of the period corresponding to the period of the ring rotations (i.e. 1/RPM). This behavior is common to all the operating conditions; the period adjusts to the ring speed. Hence, we attribute this behavior to the fact that the fins that were lost to breakage were distributed in a non-uniform manner, and thus the concentration of CO varies with the actual the number of fins in the oxidation zone at any given time. Note that the ability to observe this behavior is an indication that our efforts to minimize downstream mixing and dispersion have paid off, and we are able to discriminate changes in gas composition over a very short time scale. Note further that this behavior provides some verification of distinct oxidation and reduction zones in the system, and that the ceria is indeed responsible for the observed production of CO.

The efficiency data presented in Figure 16 is calculated using the relationship:

$$Eff = \frac{0.21\,(W/sccm\ CO) \times CO\ \ flow}{0.95 \times Q_{solar}} \times 100\%$$

where Q_{solar} was calculated from the normal incident solar radiation (also sampled at 1 second intervals), and the current attenuator position using a relationship developed with water calorimetry (see below). The 0.95 factor accounts for transmission losses as the concentrated flux passes through the quartz window enclosing the CR5 aperture. The highest instantaneous

efficiency for this condition is 0.6%, which is also among the highest observed for any condition in this data set. Efficiencies and power demands are discussed in more detail below.

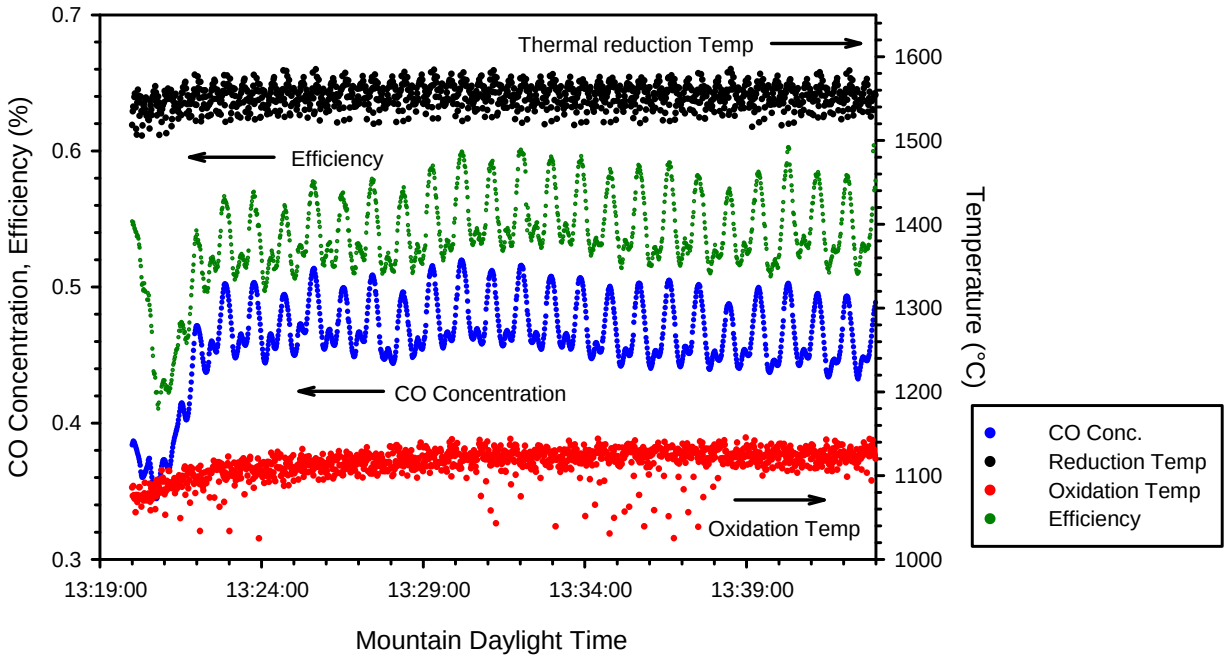

FIGURE 16. EXAMPLE OF DATA COLLECTED FOR DATA SET 2. THIS PARTICULAR PLOT CORRESPONDS TO OPERATING CONDITION 3 IN TABLE 1.

Figure 17 presents the CO production for Data Set 3. Qualitatively, the data resembles that of Data Set 2A more than 2B. That is, there is a peak for the two highest flows at the intermediate rotation speed. Consistent with the expectation of increased utilization resulting from deeper reduction at higher reduction temperature, the maximum CO yields for Data Set 3 were about double that of Data Sets 2. The oxidation temperature for each condition in Data Set 3 is plotted in Figure 18. As before, the temperatures decrease as the flow rate and the period of a rotation increases (rpm decreases) presumably for similar reasons.

Post-test inspection of the CR5 indicated that the higher temperature coupled with heating these rings for the fourth time to extreme temperatures (or fifth if one counts the 22-ring test reported earlier from which the fin segments were taken) resulted in significantly more damage to the rings and loss of individual fins. The zirconia buffers in which the fins are embedded showed signs of delamination, and a final count upon disassembly indicated that about 1/3 of the individual fins had been dislodged or lost to breakage. However, the distribution of the loss was not consistent from ring to ring, or reactor side to reactor side, suggesting that there may have been a cascade-type event, i.e. broken fins may have become situated in a manner that they interfered with the movement of other fins, resulting in breakage. In the best case a single ring lost only 19 out of 144 individual fins.

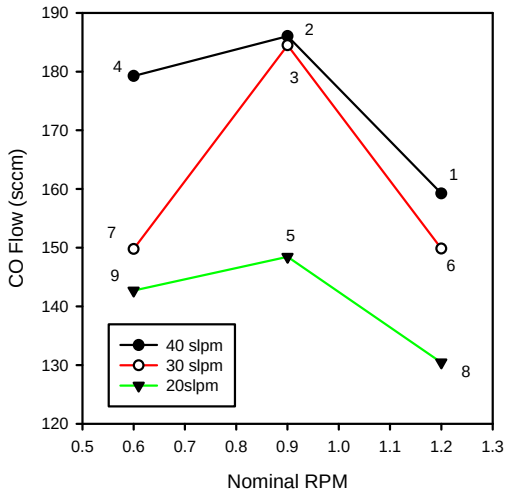

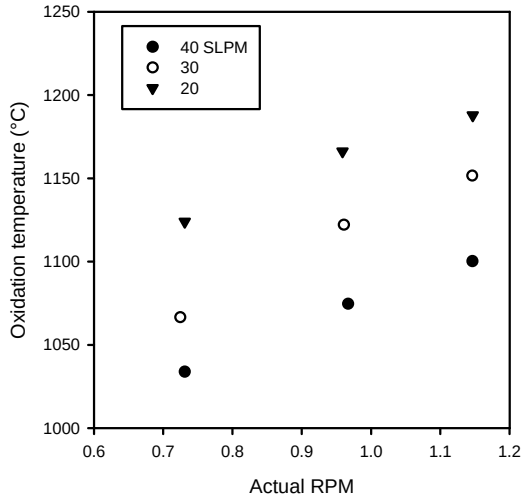

FIGURE 17. (LEFT) RATE OF CO PRODUCTION AS A FUNCTION OF CO_2 FLOW RATE AND NOMINAL ROTATION SPEED AT THERMAL REDUCTION TEMPERATURES OF 1550 °C. NUMERALS REPRESENT THE ORDER IN WHICH THE DATA WAS COLLECTED

FIGURE 18. (RIGHT) OXIDATION TEMPERATURE AS A FUNCTION OF THE ACTUAL ROTATION SPEED AND CO_2 FLOW (SHOWN IN LEGEND). Ar FLOW=21 SLPM, TR= 1550 °C.

DATA SET 4

Data Set 4 was collected with an entirely new set of 8 rings on April 6. The data points collected for this set replicated the conditions reported for Data Set 3 (thermal reduction temperature of 1550 °C), with the exception that the pressure of the reactor was allowed to float as the CO_2 flow rate was varied. To clarify, the valve upstream of the oxidation side vacuum pump was not adjusted to maintain a target pressure in the reactor. As described above (Data Set 1), allowing the pressure to float results in a near constant ratio for the flows out of the oxidation and reduction sides (e/d, in this case measured to be about 6.5:1) rather than a constant flow rate out of the reduction side as the CO_2 and hence varying ratio as the CO_2 flow rate is manipulated.

TABLE 4. OPERATING CONDITIONS FOR DATA SET 4.
THERMAL REDUCTION TEMPERATURE 1550 °C, FLOATING REACTOR PRESSURE.

Operating Condition	Ar Flow (SLPM)	CO_2 Flow (SLPM)	Nominal Ring Speed (RPM)	Observed Pressure (ATM)
1	20	20	0.9	0.25
2	20	20	0.6	0.25
3	20	40	1.2	0.39
4*	20	40	0.6	0.40
5	20	30	0.6	0.33
6	20	30	1.2	0.33
7	20	20	1.2	0.26
8	20	40	0.9	0.37
9	20	30	0.9	0.33
10*	20	40	0.6	0.40

As before, measurements of gas concentrations were redundant, with NDIR (CO, CO_2) and oxygen sensor (O_2) readings providing the principal "continuous" values, and downstream GC analyses providing the redundancy. This redundancy proved to be key as the NDIR measurements in this case were observed to diverge significantly from the GC data, and from the material balance. This was later traced to a faulty/intermittent cooling fan within the instrument. Data collected for condition 4 in particular appeared to be very unstable; operating condition 10 is a more stable duplicate of condition 4. The data from the GC was used to calibrate the NDIR data, which drifted higher over the course of the run (i.e. as the instrument temperature increased beyond specification).

During the run, two ring sections broke off but fell clear, allowing the operation to continue. (Recall each ring is composed of 6 individual sections that make up a 60° segment of the full ring.) We assume this breakage can be attributed to a few sub-par parts as is often the case for early failures.

Figure 19 shows the CO production rates as determined by GC. In the broad sense, the trends in CO yields were similar to those of Data Sets 2 and 3, i.e. higher flow rates resulted in higher yields. Overall the yields appear to be suppressed to some degree over those reported for Data Set 3. This may be result of the reduced operating pressure (oxidation kinetics are effected by CO_2 pressure), or perhaps due to differences in the two ring sets or incidental discrepancies in the operating conditions (reduction temperature) as described above. The set of oxidation temperatures (Figure 20) measured for Data Set 4 was less "well behaved" than for Data sets 2 and 3. To some extent this is related to the fact that the reduction temperatures were more variable (the set point was more difficult to maintain), but it is also likely related to differing heat transfer characteristics over the varying pressures.

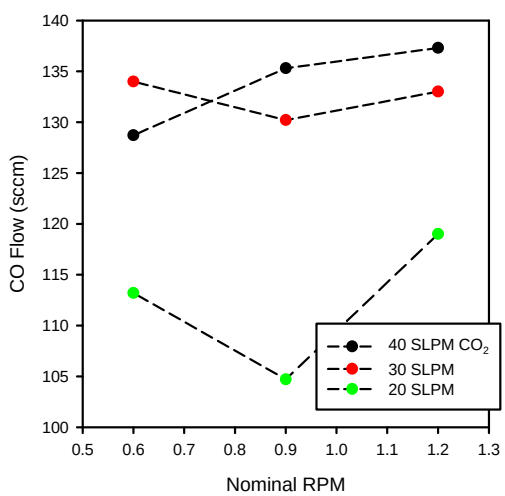

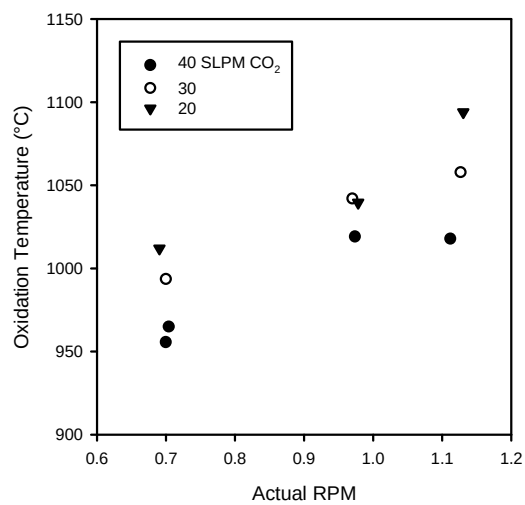

FIGURE 19. (LEFT) RATE OF CO PRODUCTION AS A FUNCTION OF CO_2 FLOW RATE AND NOMINAL ROTATION SPEED AT THERMAL REDUCTION TEMPERATURES OF 1550 °C.

FIGURE 20. (RIGHT) OXIDATION TEMPERATURE AS A FUNCTION OF THE ACTUAL ROTATION SPEED AND CO_2 FLOW (SHOWN IN LEGEND). Ar FLOW=21 SLPM, TR= 1550 °C. PRESSURE WAS ALLOWED TO FLOAT.

DATA SET 5

Following the collection of Data Set 4, the CR5 was disassembled so that the rings with missing segments could be replaced. The replacement rings were assembled from segments recovered from earlier testing. Therefore, the complement of rings used for Data Set 5 was composed of segments that had all been previously thermally cycled in the CR5. The intent was to collect a full set of data at a thermal reduction temperature of 1650 °C and a pressure of 0.5 atm. Previous experience suggested this would provide larger CO yields, but could also result in damage to the CR5. In particular, prior to this BP funded effort, extended operation at temperatures at or above this target resulted in partial melting of the inert stuffers filling the spaces on either side of the 8 rings (recall the full ring complement is 22 rings). Steps were taken during this phase of the campaign to minimize this possibility. The stuffers were rebuilt out of an insulating material with a higher thermal rating, and the aperture and stuffers were redesigned to provide a smooth transition. That is, the inert stuffers did not present a face parallel to the aperture.

As for all previous data sets, the extreme outer edges of the concentrator were shaded by vertical curtains to limit the amount of light that would be intercepted by an inert material rather than a ring. However, based on the earlier runs, the curtains were adjusted to a more open position so that the target temperatures could be reached with some headspace left for attenuator control. Also, a slower ramp up to operating temperature was utilized in order to minimize the potential for ring breakage; this extra caution was precipitated by the failure of the two segments during collection of Data Set 4. No further loss of any segments was observed during collection of Data Set 5.

TABLE 5. OPERATING CONDITIONS FOR DATA SET 5.

Operating Condition	Ar Flow (SLPM)	CO_2 Flow (SLPM)	Nominal Ring Speed (RPM)
1	20	40	1.2
2	20	30	1.2
3	20	40	0.9
4	20	40	0.6
1	N/A	N/A	N/A
1	20	40	1.2

A total of three on-sun attempts were made to collect a full Data Set at 1650 °C, the first attempt on April 26 in many ways being the most successful. The ramp-up period during this test occurred over about 4 hours total, with an extended period at 1000 °C during which adjustments were made to pyrometers. Also during the ramp, several calibration runs of the NDIR, prompted by the experience of Data Set 4, were performed. Due to this extended startup only 4 data points could be collected in the allotted time. However, in anticipation of this, an adjustment was made to the order in which data was collected so that a complete set was collected at the highest flow rate (i.e. all three rotation speeds, Table 5). The data were collected at a thermal reduction temperature of ca. 1620 °C, as the targeted 1650 °C could not be reliably maintained with the given curtain position. It appears likely that the additional concentrator area was not as efficient as expected because the beams from the outer periphery of the device pass through the aperture at a steeper angle and are

less likely to directly intercept the active ring area. The CR5 was successfully shut down after the fourth point as the intensity of incident sunlight was diminishing and clouds were forming in the vicinity of the facility.

Figure 21 illustrates the CO yields obtained during this run. This data continues the trend of increasing yield with increasing reduction temperature. Oxidation temperatures are given in Figure 22.

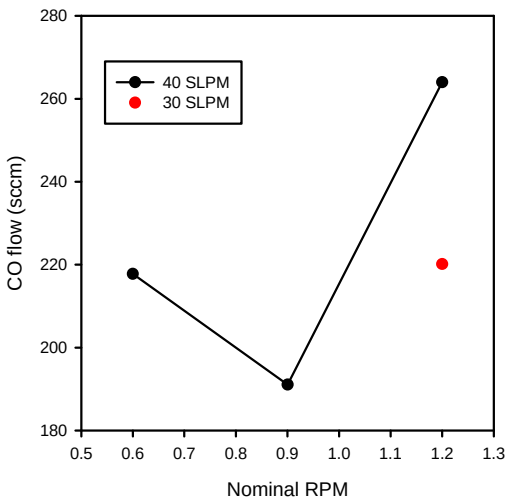

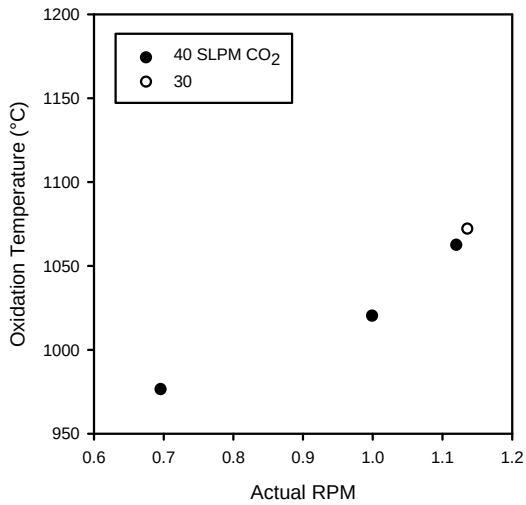

FIGURE 21. (LEFT) RATE OF CO PRODUCTION AS A FUNCTION OF CO_2 FLOW RATE AND NOMINAL ROTATION SPEED AT THERMAL REDUCTION TEMPERATURES OF 1620 °C.

FIGURE 22. (RIGHT) OXIDATION TEMPERATURE AS A FUNCTION OF THE ACTUAL ROTATION SPEED AND CO_2 FLOW (SHOWN IN LEGEND). Ar FLOW=21 SLPM, TR= 1620 °C.

Following this first run, the faulty fan on the NDIR was replaced and the electronics altered so that the fan ran continuously rather than cycled in response to a temperature signal. In addition, shading was added to provide additional shielding of the instrument from reflected sunlight. Furthermore, the curtains were positioned at an even wider condition to allow the 1650 °C mark to be reached and maintained. However other issues arose that prevented the collection of a large data set. During the first attempt on May 1, high winds arose during the first run condition. During the final attempt on May 3, a power failure related to overheating of some of the balance of system led to a loss of vacuum in the system and it had to be shut down. Only a single data point was collected; 263 sccm of CO was produced for the condition shown in Table 5. The power required to maintain the reduction temperature at 1650 °C was 10.4 kW.

SOLAR POWER DEMANDS, THERMAL BEHAVIOR, EFFICIENCIES

SOLAR CALORIMETRY

The CR5 prototype is capable of housing up to 22 rings of the current generation of fins. In order to ensure that enough ring segments were available for all the planned activities, and to facilitate rapid turnaround, Data Sets 2 – 5 were collected with only 8 rings. The 8 rings are centered in the aperture; insulating "stuffers" are used to fill the unused space on either side of the rings. There is

no obvious advantage to be gained from illuminating these inert materials with concentrated solar flux, and the potential disadvantages, namely thermally damaging the stationary material in manners up to and including melting, are significant. Therefore the outer edges of the concentrator were curtained off (shaded) to minimize the amount of energy that directly intercepts these "stuffer" materials. Flowing water calorimetry was used to characterize the solar furnace in this configuration so that an accurate measure of the thermal energy entering the CR5 is available. The results of three different calibration runs are shown in Figure 23. The first two are representative of the curtain position for Data Sets 2, 3, and 4. The second run was necessary as a snow storm occurred that washed accumulated dust from the heliostat. The third calibration is representative of the first curtain position for Data Set 5 when the reduction temperature was 1620 °C. The solar power for the final condition in Data Set 5 was inferred from the calibration and the curtain/concentrator geometries (i.e. increased by the ratio of the un-shaded areas). The available power shown in Figure 23 is actually somewhat less than would be anticipated from previous "best case" measurements and geometry alone, consistent with the considerable amount of dust currently soiling the mirrors.

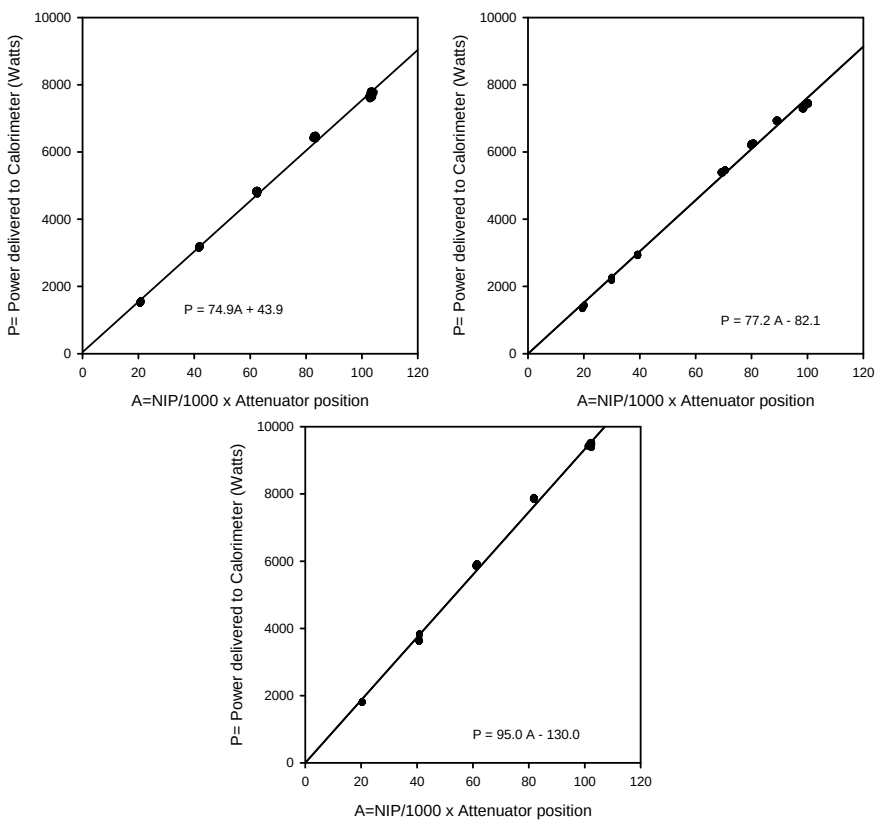

FIGURE 23. CALIBRATION CURVES FOR "SHADED' SOLAR FURNACE. TOP: DATA SETS 2-4. BOTTOM: DATA SET 5 (SEE TEXT.)

THERMAL BEHAVIOR IN DATA SETS 2-5

Above we have shown the oxidation temperatures for each individual data set. Here we examine them as a group. Figure 24 gives an example of the variability in the average reduction temperatures within a given data set. These reduction temperatures correspond to the oxidation

temperatures shown in Figure 18 for Data Set 3. The variation, while small, is unavoidable given the constantly changing resource, the ring rotation, the instantaneous variability of the temperature reading (Figure 16), and the relatively coarse control provided by the attenuator. The variability in the reduction temperature prompts us to examine the data in the form of a temperature difference ($T_{reduction} - T_{oxidation}$) rather than as an absolute value.

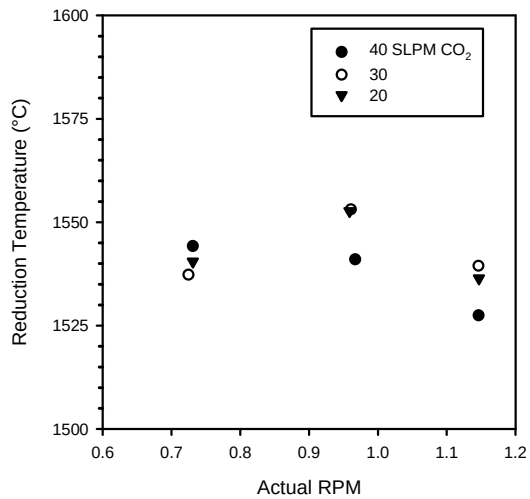

FIGURE 24. ACTUAL REDUCTION TEMPERATURES FOR DATA SET 3.

Figure 25 collects the temperature data from all 5 on-sun data sets into a single figure. In this plot we correlate the temperature difference with different a combinations of the gas flow rate and ring rotation period (1/RPM) as an initial effort towards developing a deeper understanding of the CR5 behavior. Each individual curve corresponding to a data set shows remarkably similar behavior. However, the difference between the individual curves (the y-values) should be viewed with caution. As explained above, the temperature measurements are subject to differences in pyrometer placement. Taken at face value the correlation of temperature spread with rotation and flow rate would appear to make sense. As discussed above, it is reasonable to expect that an increase in gas flow rate would result in a greater amount of heat being transferred out of the CR5 causing a decrease in the oxidation temperature (i.e., the temperature difference would increase). And as we discussed above, one might anticipate that increasing the ring rotation speed (decreasing the rotation period) would result in decreased thermal recuperation and decreased convection of heat out of the system per rotation, which would result in higher oxidation temperatures (smaller temperature difference).

Figure 26 collects the power data from 4 on-sun data sets into a single figure. Recall that power data is not available for Data Set 2A. In this case the best correlation arose when the power input required to maintain the thermal reduction temperature was plotted as a function of the total flow rate divided by the rotation period. The three Data Sets wherein pressure was maintained at a constant 0.5 atm appear to paint a coherent picture. The Data Sets were fitted with a linear regression and the results are shown on the plot. The slopes of the three Data Sets are very similar. This is consistent with the idea that the factors influencing heat transfer in the system are similar in all three cases. On the other hand, as the reduction temperature was increased, the intercepts also increase. One possible interpretation of the y-intercept is that it is representative of what the thermal losses would be in the absence of ring rotation and gas flow. In principal these would

primarily result from radiation losses from the aperture, and would be expected to increase with temperature. This interpretation is supported by the simple calculation of ratioing the temperature terms of the radiative heat transfer equation and comparing the results to the intercept ratios. For example comparing Data Sets 2B and 3:

$$\frac{(1823^4 - 298^4)}{(1723^4 - 298^4)} = 1.25; \frac{6245}{5017} = 1.24$$

And Data Sets 2B and 5:

$$\frac{(1893^4 - 298^4)}{(1723^4 - 298^4)} = 1.46; \frac{7482}{5017} = 1.49$$

Using this technique to predict a value to maintain the temperature at 1650 °C and the conditions in Table 5 gives a result of 9.6 kW (a slope of 25 was assumed, Figure 26) as opposed to the measured value of 10.4 kW. As we suggest above, the power required in excess of the prediction may result from a portion of the flux intercepting the stuffers. The 8 rings occupy only 36% of the design "capture area". However at this condition beams from over 80% of the concentrator area were entering the aperture. More detailed geometric calculations or flux mapping will provide more insight and quantification.

The correlation for Data Set 4 wherein the pressure was allowed to float (values were less than 0.5 atm) shows similar behavior to the other cases, but more scatter and a lower overall power requirement and smaller intercept than Data Set 3 with a similar reduction temperature. This somewhat complicates the interpretation and suggests that conduction of heat through the gas phase also plays a role in the baseline (no flow, no rotation) thermal losses.

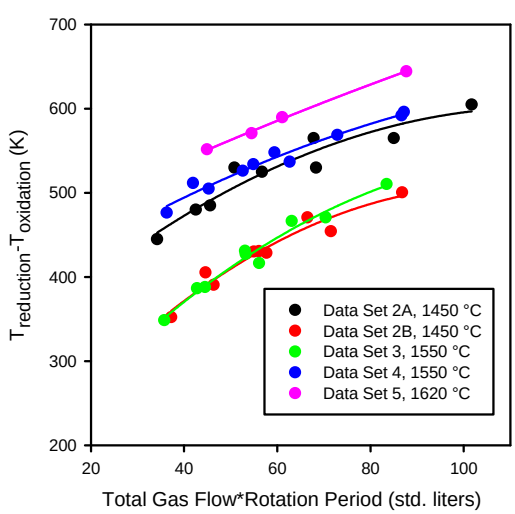

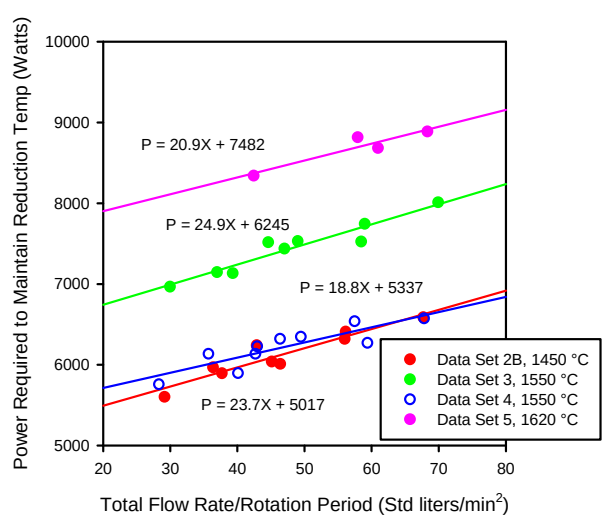

FIGURE 25. (LEFT) TEMPERATURE DIFFERENCE BETWEEN REDUCTION AND OXIDATION SIDES OF THE CR5 AS A FUNCTION OF GAS FLOW MULTIPLIED BY THE ROTATION PERIOD BY DATA SET.

FIGURE 26. (RIGHT) POWER REQUIRED TO MAINTAIN THE CR5 REDUCTION TEMPERATURE AS A FUNCTION OF GAS FLOW DIVIDED BY THE ROTATION PERIOD BY DATA SET.

As for Figure 25 the correlation in Figure 26 makes some intuitive sense. An increase in gas flow rate would result in a greater amount of heat being transferred out of the CR5 and thus the power requirement would increase. The impact of the rotation speed is less clear. More power is required as the rotation speed increases. One possible explanation is that while the heat being carried out of

the system decreases per unit rotation, the total heat being lost is increasing as the number of rotations per unit time increases. We are in the process of rationalizing our observations summarized in Figures 25 and 26 with our engineering models of the CR5.

SOLAR EFFICIENCIES

The average solar efficiencies during the steady-state periods for Data Sets 2B, 3, 4, and 5 calculated using the equation introduced above are shown in Figure 27.

$$Eff = \frac{0.21(W/sccm\ CO) \times CO\ \ flow}{0.95 \times Q_{solar}} \times 100\%$$

On examination, a few general trends are apparent. The higher flow rates typically gave higher efficiencies. In every data set, the CO_2 flow of 20 SLPM gave a lower efficiency than the to 30 and 40 SLPM cases. The data from two flow rates showed less variation within a data set. As the reduction temperature increases from 1450 °C to 1550 °C the efficiency roughly doubles (Data Set 2B vs. 3). The constant pressure condition at 1550 °C (Data Set 3) was generally better than the floating pressure at 1550 °C (Data Set 4), although as discussed above, the direct comparison is more questionable due to the change in rings. Surprisingly, increasing the reduction temperature further to 1620 °C (Data Set 5) did not result in a large across-the-board step improvement in efficiency. Although the CO yields did increase significantly, this was countered to some extent by the increased power requirement. Ideally this dynamic would be retested over the full range of flows in a system with a full ring complement where inert stuffers would not intercept any of the incident concentrated solar beam.

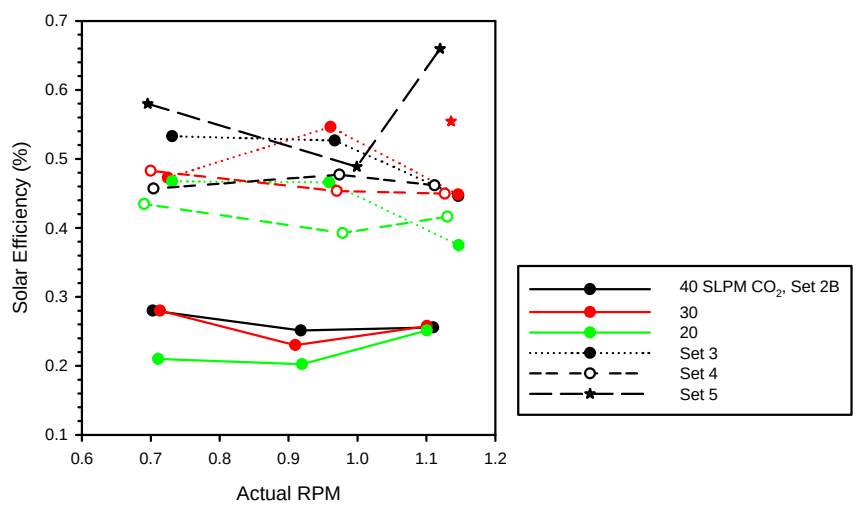

FIGURE 27. EFFICIENCY AS A FUNCTION OF CO_2 FLOW RATE AND PERIOD OF A RING ROTATION FOR DATA SETS 2B, 3, 4, AND 5.

OTHER RESOURCES

A summary of earlier work and a list of additional resources is found in the following report:

- *Final Report: Reimagining Liquid Transportation Fuels - Sunshine to Petrol*, James E. Miller, Mark D. Allendorf, Andrea Ambrosini, Ken S. Chen, Eric N. Coker, Daniel E. Dedrick, Richard B. Diver, Roy E. Hogan, Ivan Ermanoski, Terry A. Johnson, Gary L. Kellogg, Anthony H. McDaniel, Nathan P. Siegel, Chad L. Staiger, and Ellen B. Stechel – Sandia report SAND2012-0307, January 2012.

More recently published documents pertaining to metal-oxide thermochemistry include:

- *Oxygen transport and isotopic exchange in iron oxide/YSZ thermochemically-active materials via splitting of $C(^{18}O)_2$ at high temperature studied by thermogravimetric analysis and secondary ion mass spectrometry*, Eric N. Coker, James A. Ohlhausen, Andrea Ambrosini and James E. Miller – J. Matls. Chem. 22(14), 6726-32 (2012);
- *Using in-situ techniques to probe high-temperature reactions: thermochemical cycles for the production of synthetic fuels from CO_2 and water*, E.N. Coker, M.A. Rodriguez, A. Ambrosini, J.E. Miller and E.B. Stechel, Powder Diffraction, 27(02), 117-125 (2012);
- *Fuel Production from CO_2 Using Solar-Thermal Energy: System Level Analysis*, Jiyong Kim, Terry A. Johnson, James E. Miller, Ellen B. Stechel, Christos T. Maravelias – accepted for publication in Energy and Environmental Science.

ACKNOWLEDGEMENT

The work summarized in this document was funded by BP Corporation North America under a WFO agreement. The authors thank Ellen Williams of BP for her support and Daniel Cunningham our BP program manager for his many insights and contributions. The authors thank Amanda Lozoya, Kristin Meyer, David Saiz, Tim Turner, and Adrian Wagner for their efforts in fin fabrication. The authors also thank John Stuecker and his colleagues at Robocasting, LLC for their contributions to the fabrication of the ceramic parts and ring assemblies.

DISTRIBUTION:

1	MS1349	J.E. Miller, 1815 (electronic copy)
1	MS1349	W.A. Hammetter, 1815 (electronic copy)
1	MS0734	A. Martino, 6124 (electronic copy)
1	MS0899	Technical Library, 9536 (electronic copy)

Sandia National Laboratories